

GQuEST Beamsplitter Cryostat Summary

Daniel Grass^{1,*}

¹*Division of Physics, Mathematics and Astronomy,
California Institute of Technology, Pasadena, CA 91125*

(Dated: June 7, 2024)

The GQuEST (Gravity from the Quantum Entanglement of Space-Time) experiment uses tabletop-scale Michelson laser interferometers to probe for fluctuations in space-time. In order to aid this search, we are considering cooling the beam splitter to reduce some thermal noise sources. This paper will summarize my work modeling the noise's dependence on the beam splitter's temperature, the design of the cryostat, and modeling of the cryostat.

1. GOALS AND MOTIVATION

The goals for the GQuEST Beam Splitter Cryostat is primarily to reduce thermal noise in the beam splitter. These noise sources include substrate thermorefractive noise, mechanical noise, substrate thermoelastic noise, substrate charge carrier noise, and a coating thermo-optic noise. With a standing wave Michelson Interferometer (vs. a traveling wave), the strongest noise source in our measurement band (8 to 40 MHz) is substrate thermorefractive noise. With a traveling wave interferometer, this noise source can be suppressed so that the dominant noise source is the coating contribution to mechanical noise in the end mirrors, which cannot be addressed with a cryostat just on the beamsplitter. The coating noise in the beam splitter, both mechanical and thermal, will be greatly subdominant to that of the end mirrors because the end mirror coating thickness is much higher since they are high reflectors. In short, a cryostat barely reduces the noise if we use a standing wave configuration for GQuEST.

In addition to lowering the thermal noise, cooling the beam splitter can greatly reduce the light lensed by the beamsplitter into higher order modes.

Our general idea to cool an optic cryogenically is to use a cold head that connects, with thermal straps, to the optic in a vacuum chamber. The design is further designed below.

2. THERMAL NOISE AS A FUNCTION OF TEMPERATURE

In the following section, I will briefly summarize thermal noise in the beam splitter and show its dependence on temperature. This importantly includes material properties that change with temperature. Most of this section is based off [1]. See Fig. 1

2.a. Substrate Thermorefractive Noise

1. Standing Wave Interferometer

Substrate Thermorefractive (STR) Noise arises from microscopic temperature fluctuations in the beamsplitter that change the refractive index (since it has a temperature dependence), which then changes the optical path length of the transmitted arm. Mathematically [2, 3],

$$S_L^{\text{STR,sw}}(\Omega) = \frac{4k_B\kappa_s T^2 \beta_s^2}{\pi(C_s \rho_s w^2 \Omega)^2} \frac{h}{\cos(\theta_2)} \frac{\eta + \eta^{-1}}{2\eta^2} \left[1 + \frac{2k^2 w^2 \eta}{(\eta + \eta^{-1})(1 + (2kl_{\text{th}})^4)} \right]. \quad (1)$$

Here, $\eta = \frac{\cos(\theta_2)}{\cos(\theta_1)}$, $\theta_2 = \sin^{-1}(\frac{1}{n} \sin(\theta_1))$, and $l_{\text{th}} = \sqrt{\kappa_s / (C_s \rho_s \Omega)}$. See the table in the appendix for remaining definitions.

The last term in Eq. (1), which only arises in a standing wave interferometer, is quite large in our measurement band; it is equal to 1,300 at our fiducial measurement frequency of 17.6 MHz.

For the entire GQuEST measurement band, this equation can be very well approximated as white noise,

$$S_L^{\text{STR,sw}}(\Omega) \approx \frac{k_B h \lambda^2 \cos(\theta_1)}{16\pi^3 w^2} \frac{T^2 \beta_s^2}{\kappa_s (n^2 - \sin^2(\theta_1))} \quad (2)$$

The second fraction contains everything we can change by cooling the beamsplitter. At room temperature, this noise source is dominant by an order of magnitude in amplitude. However, we can make this noise source subdominant to mechanical noise in the end mirror coating by cooling to 123 K (or more):

Values for $T^2 \beta_s^2 / (\kappa (n^2 - \sin^2(\theta_1)))$ in (m K)/W:

c-Si, 294 K: $1.4 \cdot 10^{-6}$

c-Si, 123 K: $1.7 \cdot 10^{-8}$

c-Si, 77 K: $6.5 \cdot 10^{-10}$

There could be slightly more subtle behavior by using the full formula.

* dgrass@caltech.edu

2. Traveling Wave Interferometer

If a traveling wave interferometer is used, then the STR noise is

$$S_L^{\text{STR,traveling}}(\Omega) = \frac{4k_B\kappa_s T^2 \beta_s^2}{\pi(C_s \rho_s w^2 \Omega)^2} \frac{h}{\cos(\theta_2)} \frac{\eta + \eta^{-1}}{2\eta^2}. \quad (3)$$

With no approximations, the temperature dependent properties can be factored out:

$$S_L^{\text{STR,traveling}}(\Omega) = \frac{4k_B}{\pi w^4 \Omega^2} \frac{h}{\cos(\theta_2)} \frac{\eta + \eta^{-1}}{2\eta^2} \frac{T^2 \kappa_s \beta_s^2}{C_s^2 \rho_s^2} \quad (4)$$

2.b. Mechanical Noise

Mechanical Noise arises from microscopic vibrations in the coating and substrate of an optic that change the location of the reflecting surface and therefore optical path length.

1. Coating Mechanical Noise

The Coating Mechanical Noise (CMN) floor for an optic is given by

$$\overline{S}_L^{\text{CMN}}(\Omega) \approx \frac{16k_B T h_c \varphi_c}{\pi^3 M_s w^2 \Omega}, \quad (5)$$

The thickness of a coating is a function of the reflectivity of the optic. A beamsplitter needs just a few layers, so the coating layer is quite thin. Accordingly, the coating mechanical noise is around 10 times smaller in power in the beamsplitter than the end mirrors for all frequencies.

I don't know about the temperature dependence of the material properties of Ta₂O₅, but in general coating mechanical noise should just scale linearly with temperature.

2. Substrate Mechanical Noise

The Substrate Mechanical Noise (SMN) floor for an optic is given by

$$\overline{S}_L^{\text{SMN}}(\Omega) \approx \frac{16k_B T h}{\pi^3 v_s^2 \rho_s w^2 Q_s \Omega} = \frac{16k_B T h \varphi_s}{\pi^3 M_s w^2 \Omega}. \quad (6)$$

The beam splitter substrate mechanical noise should be very similar to that of the end mirrors. The beamsplitter has a 1.5 times larger diameter than the end mirrors so it has a higher transverse mode cutoff frequency, but overall the substrate mechanical noise in the beamsplitter will be equal to or less than the end mirrors.

A cooler optic may have lower substrate mechanical noise due to a higher quality factor, as Akheizer damping, the dominant loss in the GQuEST measurement band, is proportional to temperature. If the dominant loss is clamping loss, then the change in total quality factor is minimal. Other relevant material properties are pretty invariant with temperature.

2.c. Substrate Thermoelastic Noise

Substrate Thermoelastic (STE) noise arises from random fluctuations in temperature that result in the thermal expansion of all the optics (not just the beamsplitter). The power spectral density of substrate thermoelastic (STE) noise in our measurement band is [4],

$$S_L^{\text{STE}}(\Omega) = \frac{8}{\sqrt{2\pi}} \frac{k_B \kappa_s T^2 \alpha_s^2 (1 + \nu_s)^2}{C_s^2 \rho_s^2 w^3 \Omega^2}. \quad (7)$$

Since this noise is also in the end mirrors, cooling the beam splitter will at most reduce the overall STE noise by a factor of 1/3 in power.

2.d. Coating Thermo-Optic Noise

Coating Thermo-Optic (CTO) Noise arises from microscopic temperature fluctuations in the optic coating changing the optical path length. Coating Thermo-Optic Noise is made up of Coating Thermoelastic Noise (CTE) and Coating Thermorefractive Noise (CTN). For the GQuEST measurement band, they are incoherent and therefore add in quadrature.

The PSDs of CTE and CTR noise are [5–7]

$$S_L^{\text{CTE}}(\Omega) = \frac{2\sqrt{2}k_B T^2 \Gamma_{\bar{\alpha}}(\Omega)}{\pi w^2 \sqrt{\kappa_c \rho_c C_c \Omega}} \left(\bar{\alpha}_c h_c - \bar{\alpha}_s h_c \frac{C_c}{C_s} \right)^2, \quad (8)$$

$$S_L^{\text{CTR}}(\Omega) = \frac{2\sqrt{2}k_B T^2 \Gamma_{\bar{\beta}}(\Omega)}{\pi w^2 \sqrt{\kappa_c \rho_c C_c \Omega}} (\bar{\beta}_c \lambda)^2, \quad (9)$$

The asymptotic forms (i.e. at low and high frequencies) of the cut-off parameters for the CTE and CTR contributions, respectively, are

$$\Gamma_{\bar{\alpha}}(\Omega) = \frac{1}{\mathcal{O}(1 + R(1 + R)h_c^2/r_T^2)}, \quad \Gamma_{\bar{\beta}}(\Omega) = \frac{1}{\mathcal{O}(1 + 2\bar{\lambda}^2/r_T^2)}, \quad (10)$$

where $R = \sqrt{\kappa_c \rho_c C_c / \kappa_s \rho_s C_s}$, $\bar{\lambda}$ is defined below, and the other variables are defined above.

$$I(z > 0) \propto e^{-z/\bar{\lambda}} \quad \bar{\lambda} = \frac{\lambda}{8 \ln(n_H/n_L)} \left(\frac{1}{n_L} + \frac{1}{n_H} \right) \quad (11)$$

Coating Thermo-Optic Noise is proportional to Temperature squared. I don't know about the temperature dependence of the material properties of Ta₂O₅. KAGRA papers

claim CTO Noise drops a lot at low temperatures, likely due to this T^2 dependence, but they don't cite or calculate anything.

Coating Thermorefractive noise has no dependence on the thickness of the optic, so its contribution from the beam splitter is just as large as that from the end mirrors.

I am currently reformulating the theory of coating thermorefractive noise. These equations may change.

2.e. Substrate Charge Carrier Noise

Substrate Charge Carrier (SCC) Noise has a similar mechanism to Substrate Thermorefractive noise, but it is the density of electrons, not temperature itself, that fluctuates and creates a noise source. The exact form of SCC Noise is

$$S_L^{\text{SCC}}(\Omega) = \frac{2D\alpha_e^2 N_0 h}{\pi\omega^2} \left(\left[\frac{2k^2}{\Omega^2 + (4Dk^2 + D/l_D^2)^2} \right] + \left[\frac{3}{w^2(\Omega^2 + (D/l_D^2)^2)} \right] \right). \quad (12)$$

The second fraction's is much smaller than the first's above 77 K, so

$$S_L^{\text{SCC}}(\Omega) \approx \frac{4Dk^2\alpha_e^2 N_0 h}{\pi\omega^2} \left[\frac{1}{\Omega^2 + (4Dk^2 + D/l_D^2)^2} \right]. \quad (13)$$

$2\pi(4Dk^2 + D/l_D^2) \approx 200$ GHz, so we can further approximate SCC Noise as

$$S_L^{\text{SCC}}(\Omega) \approx \frac{4k^2\alpha_e^2 N_0 h}{\pi\omega^2 D} \left[\frac{1}{(4k^2 + 1/l_D^2)^2} \right]. \quad (14)$$

2.f. Beam Splitter Transfer Function

the measured noise at the interferometer output is modulated by the transfer function for phase modulations imparted at the beamsplitter $H(\Omega) = \cos^2(\Omega L/c) \leq 1$. This antenna function originates from the phase modulation on the transmitted beam destructively interfering with the unmodulated reflected beam at the output port if $\Omega c/2L$, where L is the length of the interferometer arms. Thus, the total beam splitter noise measured is $H(\Omega) S_L^{\text{BS noise}}(\Omega)$

3. THERMAL LENSING

The fractional power lensed by the beamsplitter out of the TEM00 mode is given by

$$\Lambda_{\text{defect}} = 0.07\eta \left(\frac{\beta_s}{\kappa\lambda} (\Lambda_c + \Lambda_s) P_{\text{BS}} \right)^2, \quad (15)$$

In terms of what the beam splitter cryostat can address, the power lensed out of the TEM00 mode is proportional to $(\beta_s/\kappa_s)^2$. Going from room temperature to 40 K reduces the power lensed by 10^6

4. MATERIAL PROPERTIES AS A FUNCTION OF TEMPERATURE

Here are some graphs of the material properties of silicon with a strong temperature dependence. See Figs. 2 and 3.

5. CRYOSTAT DESIGN

In this section we detail the considerations and choices for the proposed design of the cryostat.

5.a. Design Choices

The first consideration when designing a cryostat is the target temperature. If we use a standing wave Michelson interferometer, the goal of the cryostat is to make Substrate Thermorefractive Noise subdominant. Thus, the target temperature is around 80 K. The design (in terms of materials, cold head selection, number of layers of thermal shields, etc) remains mostly the same between 40 K and 123 K. Basing my designs of the QIL Megastat, there is an external cold head with a cold finger that goes between the cold head and the central vacuum chamber. This cold finger is then connected to a cold breadboard which holds the beamsplitter mount and beamsplitter. Because our measurement band is in the MHz, we don't have to worry as much about vibration compared to BBH/BNS merger detectors and thus have a rigid mirror mount instead of suspending the mirror. For some overview photos, see Fig. 4, Fig. 5, and Fig. 6.

5.b. Minimizing Vibration

All cold heads vibrate, and this vibration should be minimized to make locking the cavities easier and achieving a low amount of light leaving the interferometer (contrast defect). Thus, the Cryomech PT30RM was selected, as pulse tubes, especially those with a remote motor, have the lowest vibration compared to GM Coolers or Sterling Coolers. The cold head to cold finger linkage is a loose copper strap from TAI which has high thermal conductivity but doesn't transmit vibrations as much as a rigid connection. The cold finger is connected to the breadboard with

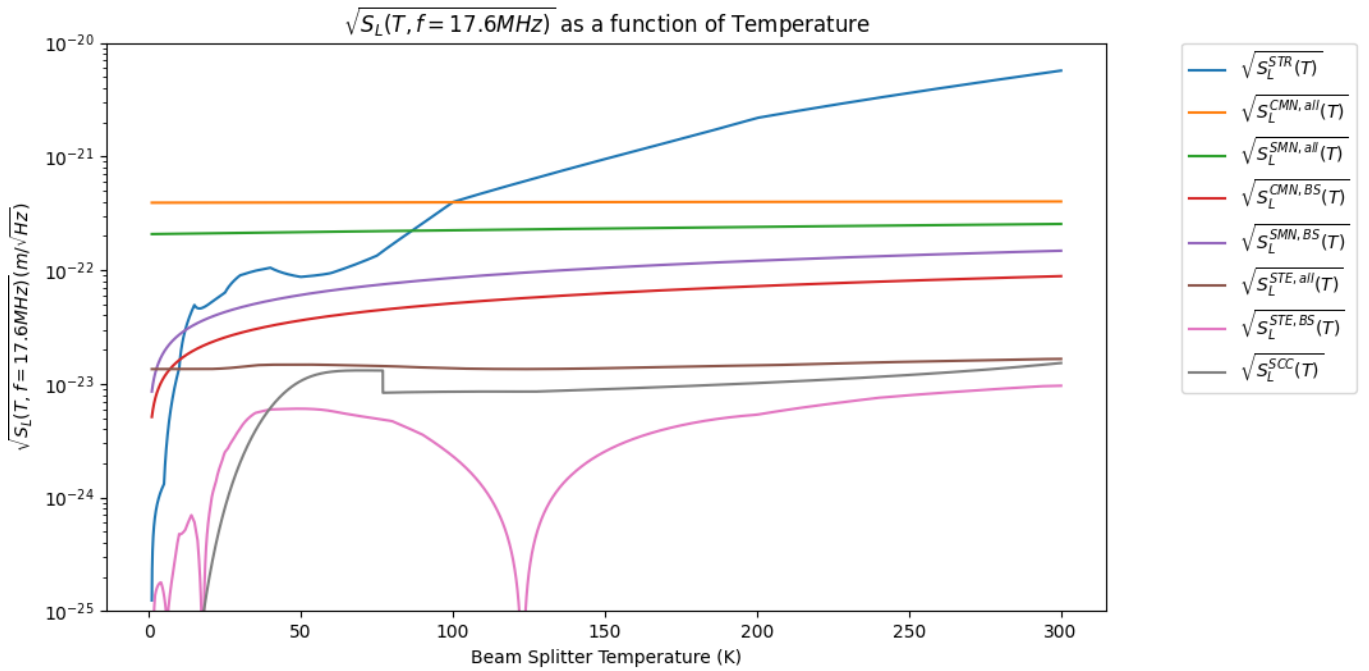


FIG. 1: Noise, ignoring beam splitter transfer function since the interferometer arm length is not set at this time

thermal straps as well. The whole PT30RM (except the remote motor) is attached to the vacuum system via bellows to reduce vibrations on the vacuum components. The PT30RM is then supported via T-Slotted Framing (80/20) so that vibrations go into the ground. The breadboard could be supported with viton spheres instead of being rigidly screwed to the PEEK supports, but that is not designed or planned for now. Fig. 7 and Fig. 8 are images that show this design.

5.c. Supports and Reducing Conduction

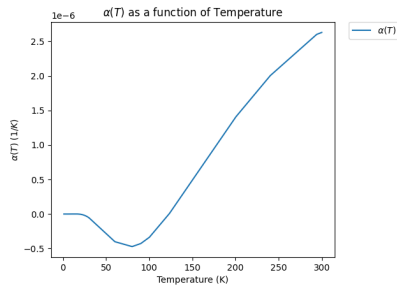
Reducing the thermal load, i.e. the amount of power that leaks into the thermal bath, is important to achieve the desired temperature quickly. In vacuum, there is no convection, so the two methods of heat transfer are conduction and radiation. To reduce conduction to the room temperature vacuum chamber, 3 custom PEEK rods are each used to support the breadboard, the cold finger, and the thermal shields (which reduce radiation loss), respectively. PEEK is an ideal choice as it is UHV compatible, a thermal insulator, strong, and machinable. Conduction is proportional to $\Delta T/L$, where ΔT is the difference in temperature and L is the length of the conductor. Because ΔT is roughly the same between the thermal shields and the vacuum chamber, as they are radiatively coupled (the radiative power transferred has T^4 scaling), increasing the length L is more impactful than decreasing ΔT . Thus, all the supports go directly to the vacuum chamber. See Fig. 9.

5.d. Reducing Radiation

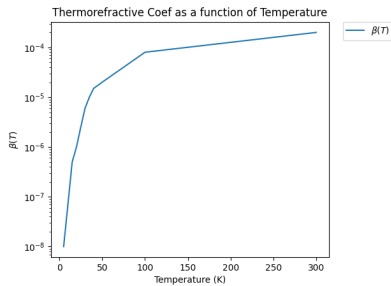
Two layers of aluminum thermal shields (page 6) reduce the radiative load. Aluminum is an ideal choice because it is UHV compatible, has a low emissivity, light weight, strong, and machinable. The radiation load reduction goes as $1/(n+1)$, where n is the number of shields. 1 layer will likely be sufficient, but 2 layers allow for the inside to get colder faster. In addition, the inner layer might be cooled, making one effective layer of thermal shielding. Both layers of shields are octagonal design with an octagonal bottom, 8 panels, and an octagonal top. An octagon geometry was chosen as the central vessel has 8 equally spaced ports. All of the PEEK supports go through the bottom layers of shield. The shields are designed to be easily removed, except the bottom. The panels have port holes and tapped holes to allow for laser light, electronics, etc to get through and to allow covers, heaters, etc to be attached. Any combination of layers is possible (no shields, just inner, just outer, or both). See Fig. 10

5.e. Maintaining Stable Temperature and Heating to Room Temperature

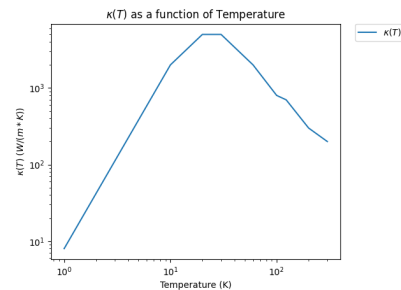
To keep a stable temperature and to raise the temperature up to room temperature quickly, heaters are used on the beam splitter mount, on the breadboard, and on each layer of shielding. The breadboard heater is used to cancel unneeded cooling at equilibrium and is placed by the cold finger to reduce thermal gradients. The cold head cannot be turned on and off easily. The heater on the beam



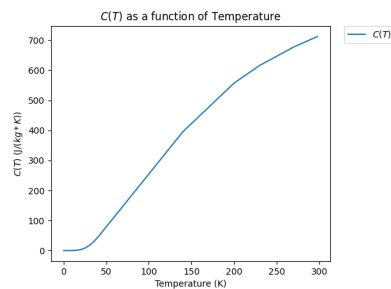
(a) Coef of Thermal Expansion



(b) Thermorefractive Coef



(c) Thermal Conductivity



(d) Heat Capacity

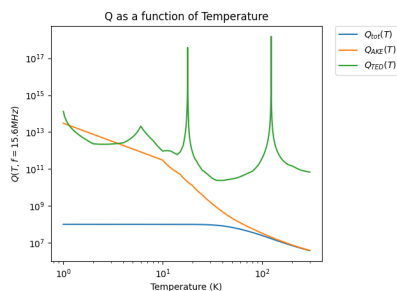
(e) Quality Factor. Note that a somewhat arbitrary anchor damping of 10^8 is added since a Q of 10^{11} seems unrealistic

FIG. 2: Silicon Material Properties as a Function of Temperature

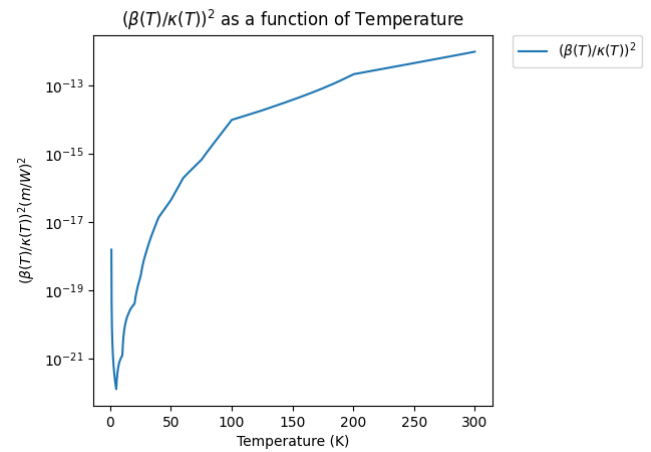


FIG. 3: Power Lenses is Proportional to the Quantity Graphed

splitter mount is used to maintain a stable temperature with PID control. Thermistors are placed around the beam splitter, on the cold plate, on each layer of shielding, and near the cold head to monitor the temperature.

5.f. Cold Finger Connection Design

The cold finger is a copper bar with a 1 inch by 1 inch cross section and attaches to the cold head in a 6 way UHV cross. The top of the 6 way UHV cross has the cold head, the bottom supports the cold finger, the sides allow for assembly, the front is attached to the central vessel with the beam splitter, and the back has a multi-port reducer flange. This flange has a thermistor, a pressure gauge, a pump, and a blowout valve. A pressure gauge is important because this volume is far away from the vacuum pumps unless a pump is connected. A pump is not needed unless this area is sealed from the rest of the interferometer. This area would need to be sealed if the interferometer had to be baked out in situ while keeping the cold head separate since it cannot be baked out. A blowout valve is necessary to avoid over-pressurizing the vacuum chamber and making a bomb. See 7, 8, and Fig. 11

5.g. Condensation on Optics Mitigation

An issue with cold optics is condensation, mostly water, building up over time. There are a few possible mitigation strategies. The first is to bake out the vacuum chamber under vacuum before cooldown so that water will not condense on the beam splitter. The second is to physically prevent water from being released and condense on the optic. This can be done by adding cold barriers (metal plates work here) that don't release water but do absorb it from room temperature sources. These can be mounted

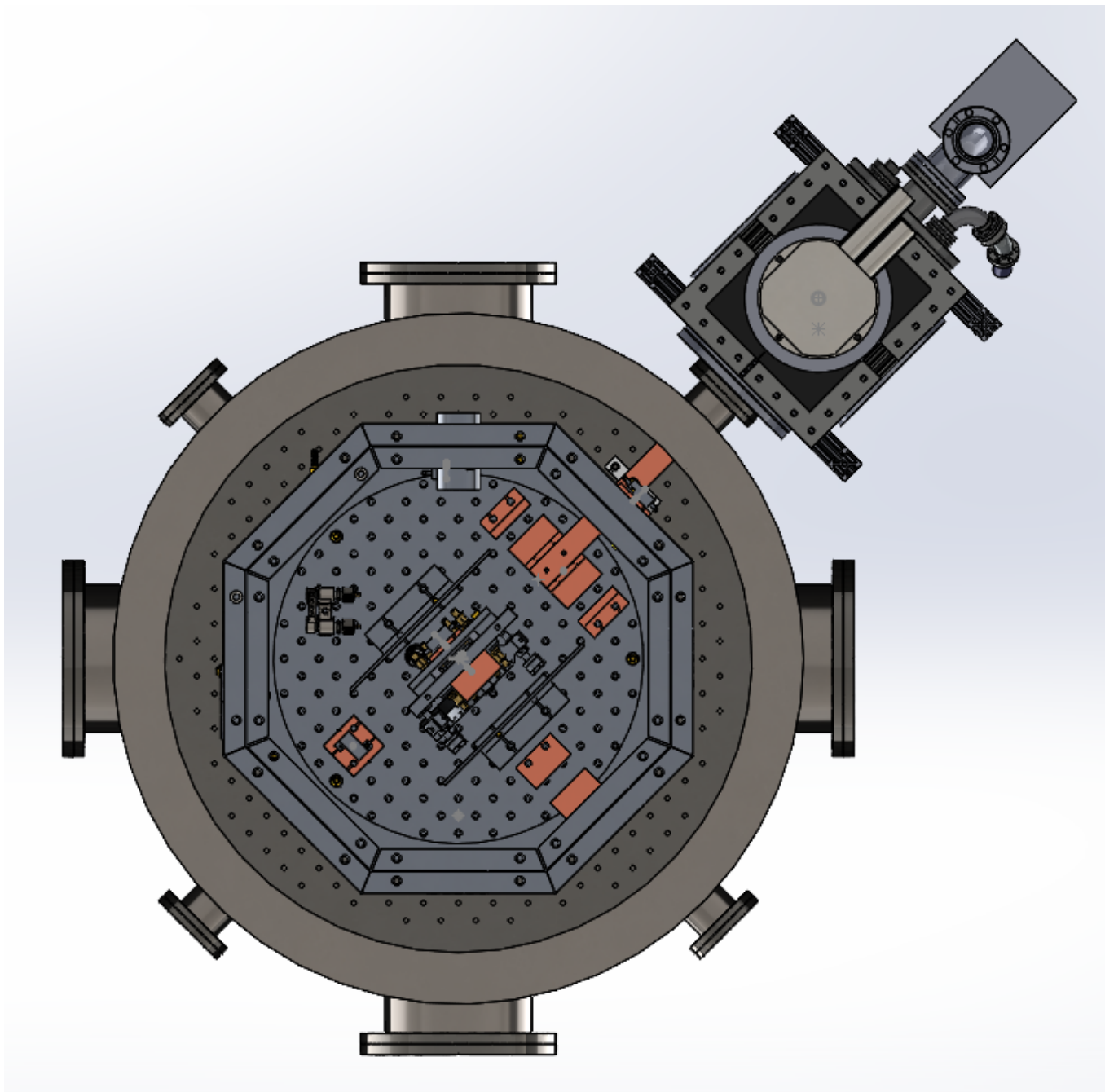


FIG. 4

on the cold plate, or the entire inner shield can be made cold. The third strategy is to remove the water from the beamsplitter, either by periodically heating it up or by radiatively heating it, for example with microwaves.

5.h. Thermal Reservoir Backup Strategy

In case the vibration of the PT30RM is too large to allow measurements with the cold head turned on, a cheap and (hopefully) easy to implement backup strategy is to use a thermal reservoir. In this scenario, the cold head would charge this reservoir by cooling it down to 30 K and the remaining material to their intended equilibrium temperature. The cold head would then be switched off and the reservoir would slowly take in the heat that leaks into the breadboard. After a while, the reservoir would have to be cooled again as it heats up. Another more expensive strategy is to use a sorption fridge.

5.i. Fasteners

Brass screws and Belleville washers, while not necessarily needed everywhere, are planned. These are used to ensure screwed joints stay tight after thermal contractions.

5.j. Product Selection

The PT30RM is the best overall choice for its base temperature, low vibration, and HV (nearly UHV) compatibility. Other possible products are the Sumitomo CH-110, which has more vibration but a lot more cooling power. A list of options is on the DCC (C2300004). Many of the vacuum parts would be sourced from Kurt J Lester, like the 6 way cross and reducer flanges. Custom parts, like the shields, would be sourced from Hubs as they are the cheapest option with a wide variety of machining services and materials. TAI straps are used as well. A good candidate for the heaters is the HSA25100RJ. The temperate can be monitored and controlled with an SRS CTC100 Cryogenic Temperature Controller. This model only allows for 4 temperature inputs.

6. MODELING

I have modeled the thermodynamics of the cryostat. My goal is to get quantitative predictions for cool down time as a function of the shielding layers and cryocooler type. I also modeled the warm up time.

I primarily used Mathematica to model the thermodynamics of the cryostat. The system is broken up into 4 subsystems: the outer shield, the inner shield, the breadboard/beam splitter, and the cold finger. I include all of the radiative and conductive links between these elements, to the room temperature vacuum chamber walls, and to different models of cold head. The cold head has a cooling power (“lift”) as a function of temperature. Most links are analytically derived from first principles with one exception; the conductive links to the vacuum chamber were modeled in SolidWorks and analytically interpolated for different links; they agree with rough analytic models.

To model the cool down time, I start everything at room temperature and cool the beam splitter to its target temperature. I do this for various configurations of shielding and for different cold head models and write the cooling time into a table. I also list out the power going through each link at equilibrium and the total power going into the bath. At 123 K, it is around 5 to 13 W depending on the configuration.

For the PT30RM, it takes around 16 hours for the beam splitter to get to 123 K. Ideally, this process can occur overnight. See Fig. 12 and Fig. 13

I have also modeled the time it takes to heat everything up. With 10 to 20 W of heating power each on the breadboard, inner shield, and outer shield, it will take a day to heat everything up over the dew point. The dew point is the minimum temperature the optics can be exposed to air to avoid condensation. Without heating, it takes over a week to heat everything up past the dew point.

7. CONCLUSION

Overall, I have laid out the motivations and design for the GQuEST Beamsplitter Cryostat. I think that there is not a compelling case to build the cryostat as it will take a lot of time and money and reduce the duty cycle of the experiment. If a traveling wave interferometer weren’t used, then I would suggest this cryostat be built to reduce the total classical noise by an order of magnitude. A future version of GQuEST that had a lower classical noise floor and higher circulating laser power should consider a cryostat for the beam splitter and end mirrors.

8. ACKNOWLEDGEMENTS

I would like to thank Sander Vermeulen for reading over this summary and providing very helpful edits and Stephen Appert, Radhika Bhatt, and Nick Hutzler for helping me with the design and modeling.

[1] S. M. Vermeulen, T. Cullen, D. Grass, I. A. O. MacMillan, A. J. Ramirez, J. Wack, B. Korzh, V. S. H. Lee, K. M. Zurek,

C. Stoughton, and L. McCuller, Photon counting interferometry to detect geotropic space-time fluctuations with gquest

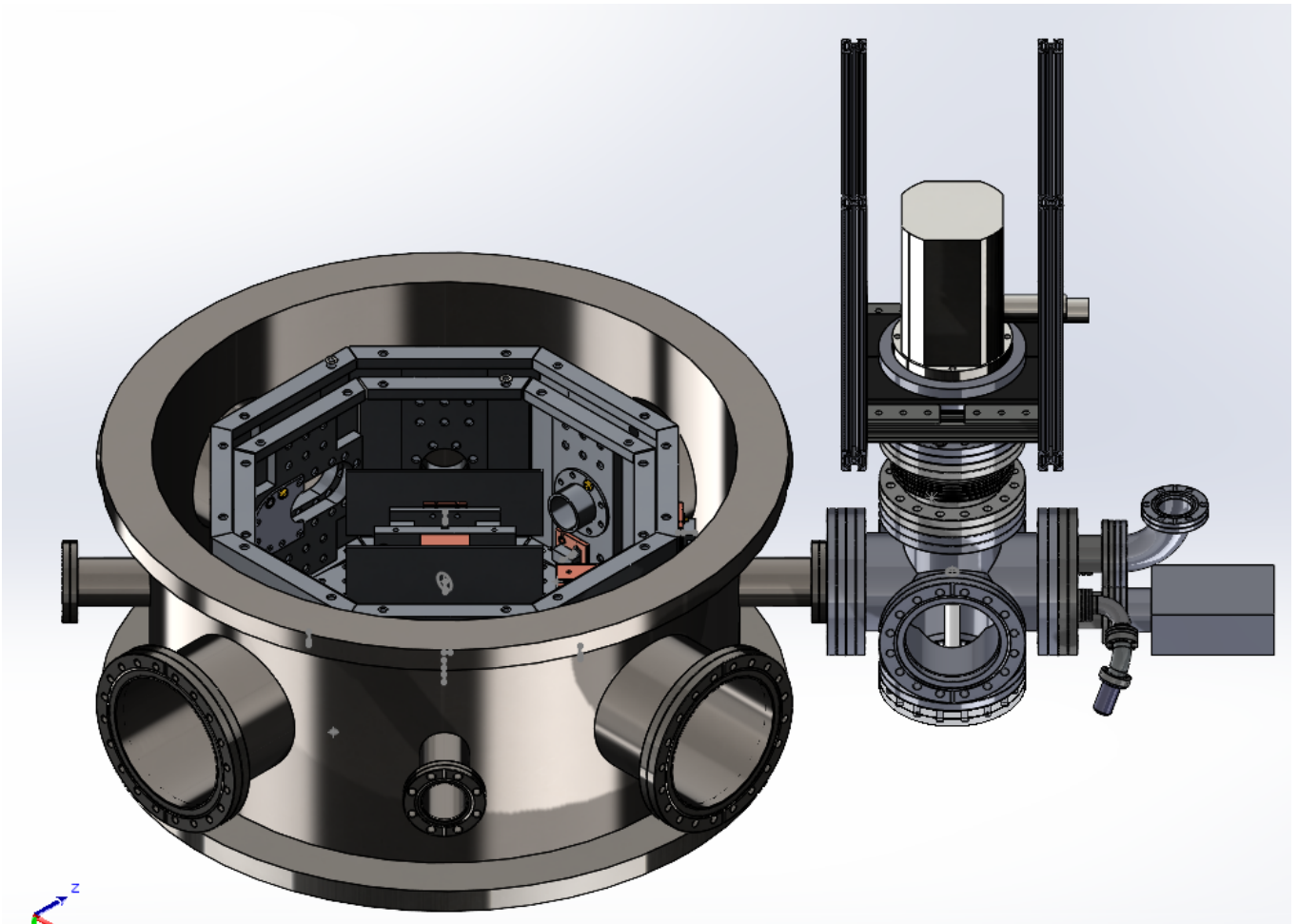


FIG. 5

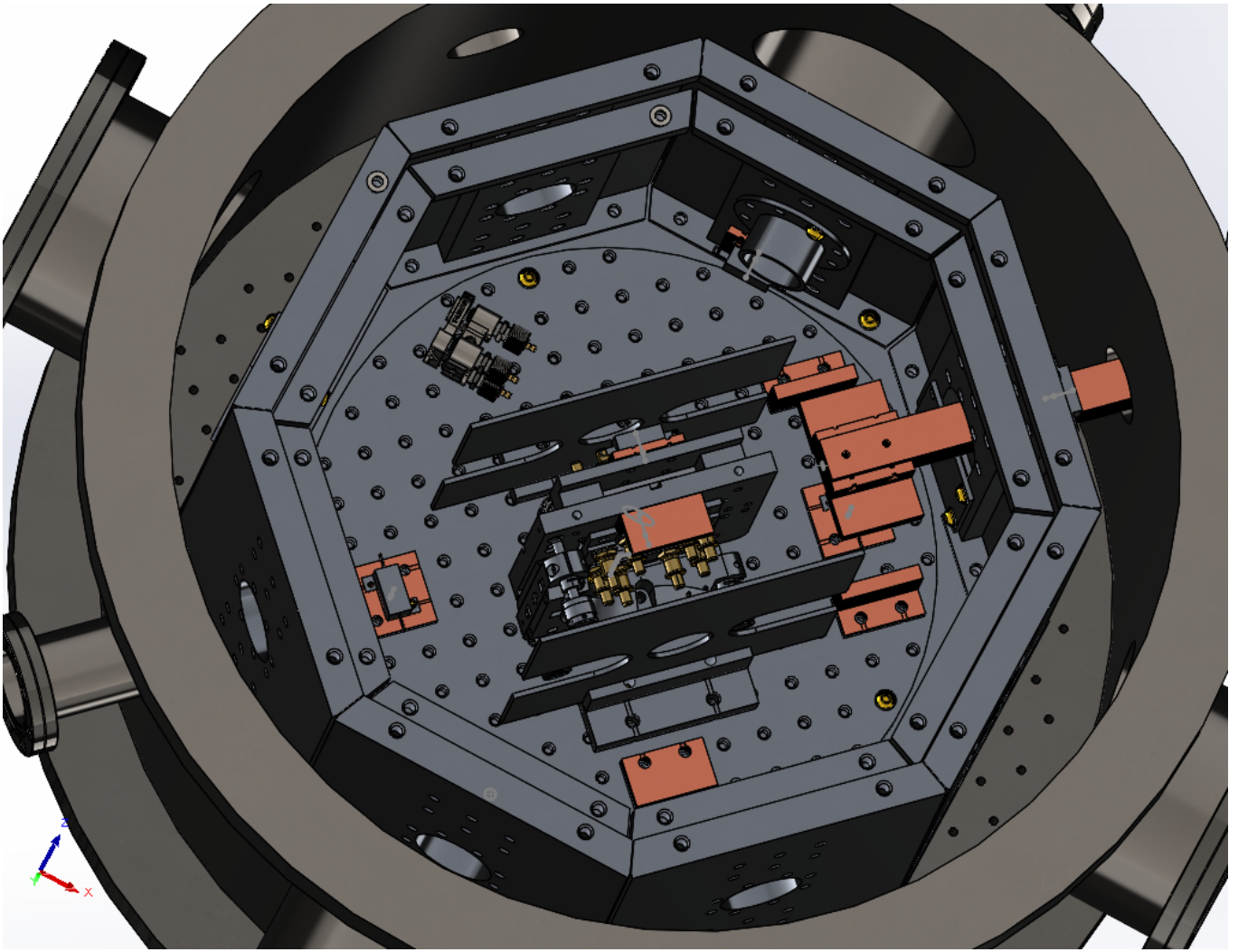


FIG. 6

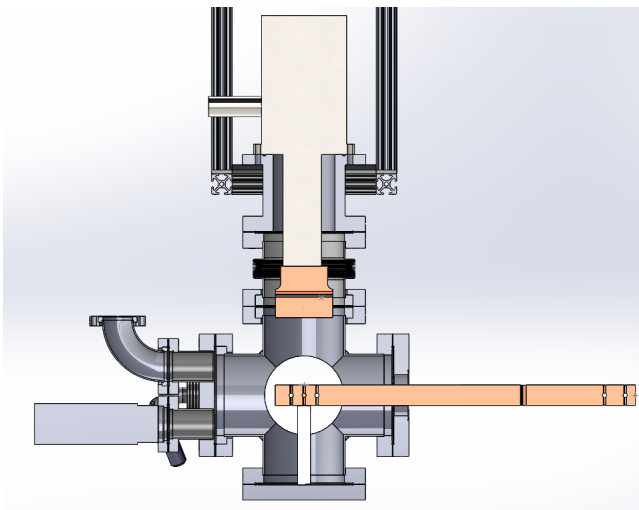


FIG. 7

(2024), [arXiv:2404.07524 \[gr-qc\]](https://arxiv.org/abs/2404.07524).

- [2] V. B. Braginsky and S. P. Vyatchanin, Corner reflectors and quantum-non-demolition measurements in gravitational wave antennae, *Physics Letters A* **324**, 345 (2004).
- [3] B. Benthem and Y. Levin, Thermorefractive and thermochemical noise in the beamsplitter of the geo600 gravitational-wave interferometer, *Phys. Rev. D* **80**, 062004 (2009).
- [4] V. Braginsky, M. Gorodetsky, and S. Vyatchanin, Thermodynamical fluctuations and photo-thermal shot noise in gravitational wave antennae, *Physics Letters A* **264**, 1 (1999).
- [5] V. B. Braginsky, M. L. Gorodetsky, and S. P. Vyatchanin, Thermo-refractive noise in gravitational wave antennae, *Physics Letters A* **271**, 303 (2000).
- [6] V. B. Braginsky, M. L. Gorodetsky, and S. P. Vyatchanin, Thermodynamical fluctuations and photo-thermal shot noise in gravitational wave antennae, *Physics Letters A* **264**, 1 (1999).
- [7] M. Evans, S. Ballmer, M. Fejer, P. Fritschel, G. Harry, and G. Ogin, Thermo-optic noise in coated mirrors for high-precision optical measurements, *Physical Review D* **78**, 102003 (2008).

TABLE I: Additional parameters of the fiducial IFO design. Material parameters are evaluated at room temperature.

PARAMETER	SYMBOL	VALUE
Laser wavenumber	k	$4 \cdot 10^6 \text{ m}^{-1}$
Input laser white phase noise PSD	$\overline{S}_{\text{in}}^{\text{LP}}$	$(10^{-7} \text{ rad}/\sqrt{\text{Hz}})^2$
Nominal filter offset frequency/readout frequency	ϵ_r	17.6 MHz
Minimum practical filter offset frequency	ϵ_r^{min}	8 MHz
Maximum practical filter offset frequency	ϵ_r^{max}	40 MHz
End mirror reflectivity	R_{EM}	≥ 0.9999
Power-recycling mirror transmissivity	T_{PR}	500 ppm
Total (round-trip) fractional power loss	Λ_{tot}	$\mathcal{O}(10)$ ppm
End mirror $1/e^2$ (2σ) intensity beam radius	w	3 mm
End mirror diameter	d	25.4 mm
End mirror thickness	h	2 mm
End mirror substrate material	c-Si	294K crystalline Si
Beamsplitter $1/e^2$ (2σ) intensity beam radius	w	3 mm
Beamsplitter diameter	d_{BS}	38.1 mm
Beamsplitter thickness	h	2 mm
Beamsplitter substrate material	c-Si	294K crystalline Si
Beamsplitter light incident angle	θ_1	45°
c-Si Density	ρ_s	2329 kg m^{-3}
c-Si Young's modulus	E_s	156 GPa
c-Si Poisson ratio	ν_s	0.265
c-Si body wave quality factor (at ϵ_r)	Q_s	$\mathcal{O}(10^6)$
c-Si Thermal conductivity	κ_s	$380 \text{ W m}^{-1} \text{ K}^{-1}$
c-Si Specific heat	C_s	$710 \text{ J kg}^{-1} \text{ K}^{-1}$
c-Si thermorefractive coefficient $\partial n/\partial T$ at λ	β_s	$2 \cdot 10^{-4} \text{ K}^{-1}$
c-Si Coefficient of thermal expansion	α_s	$2.5 \cdot 10^{-6} \text{ K}^{-1}$
c-Si Refractive index at λ	n	3.48
c-Si Diffusion constant	D	$3.76 \cdot 10^{-3} \text{ m}$
c-Si Debye length	λ_D	$4.33 \cdot 10^{-7} \text{ m}$
c-Si Mean carrier density	N_0	$< 10^{18} \text{ m}^{-3}$
c-Si Optical absorption coefficient	α_e	$1.2 \cdot 10^{-26} \text{ m}^{-3}$
c-Si Fractional power absorption at λ	Λ_{Si}	$2 \cdot 10^{-4} \text{ m}^{-1}$
Fractional BS coating power absorption (assumed)	Λ_c	3 ppm
Fractional BS substrate power absorption	Λ_s	0.4 ppm
Coating material	-	Ta ₂ O ₅ – SiO ₂
Coating thickness	h_c	$\mathcal{O}(10) \mu\text{m}$
Ta ₂ O ₅ Young's modulus	E_{Ta}	120 GPa
SiO ₂ Young's modulus	E_{SiO_2}	70 GPa
Ta ₂ O ₅ Poisson ratio	ν_{Ta}	0.29
SiO ₂ Poisson ratio	ν_{SiO_2}	0.19
Coating body wave quality factor (at ϵ_r) (derived)	Q_c	1400
Coating thermal conductivity (average)	κ_c	$2.6 \text{ W m}^{-1} \text{ K}^{-1}$
Coating density (average)	ρ_c	5200 kg m^{-3}
Coating specific heat (average)	C_c	$360 \text{ J kg}^{-1} \text{ K}^{-1}$
Coating effective coefficient of thermal expansion	$\bar{\alpha}_c$	$6 \cdot 10^{-6} \text{ K}^{-1}$
Coating effective thermorefractive coefficient	$\bar{\beta}_c$	$8 \cdot 10^{-6} \text{ K}^{-1}$
c-Si Effective coefficient of thermal expansion	$\bar{\alpha}_s$	$6.4 \cdot 10^{-6} \text{ K}^{-1}$
Coating stress	σ_c	0.5 GPa
Fused silica thermal conductivity	κ_{FS}	$1.38 \text{ W m}^{-1} \text{ K}^{-1}$
Fused silica thermorefractive coefficient at λ	β_{FS}	$8.5 \cdot 10^{-6} \text{ K}^{-1}$
Fused silica fractional power absorption at λ	Λ_{FS}	10^{-4} m^{-1}

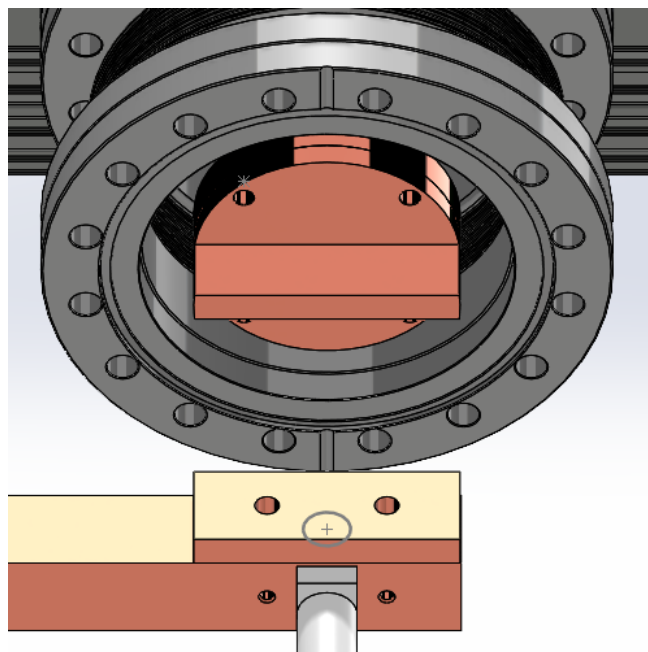


FIG. 8

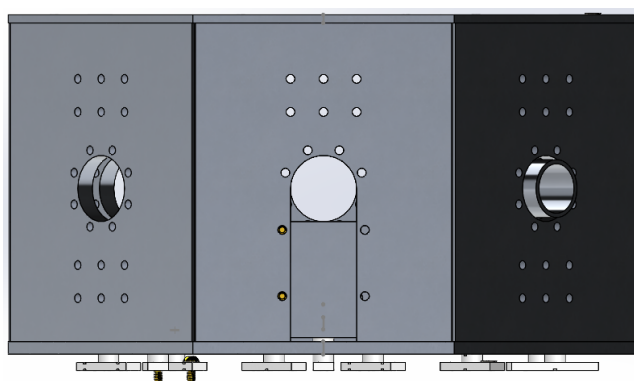


FIG. 10

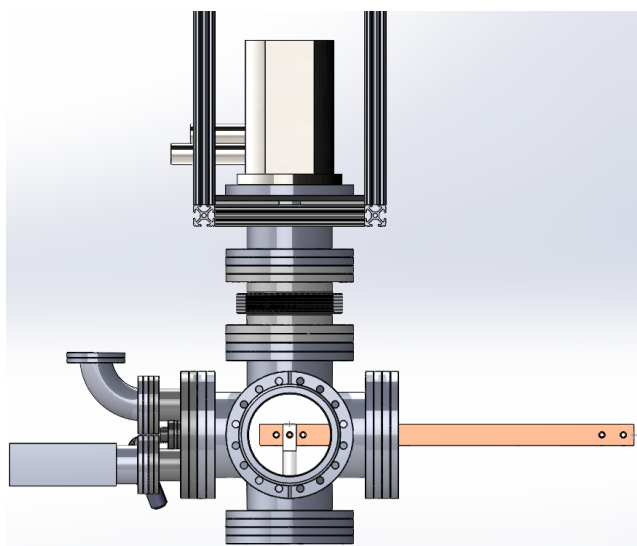


FIG. 11

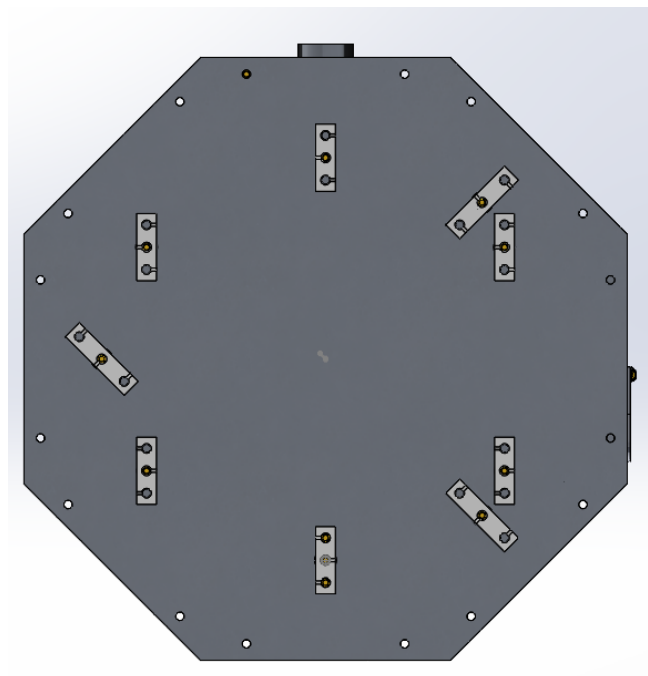


FIG. 9

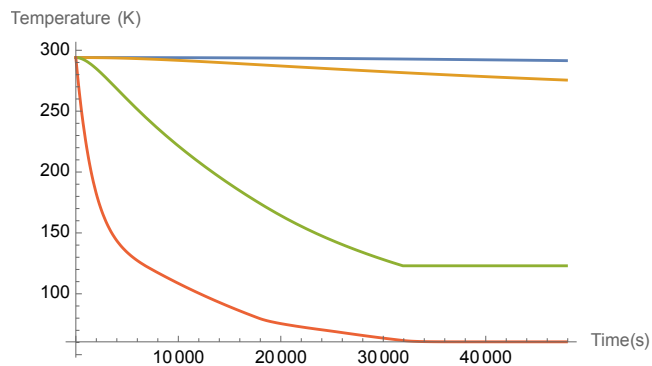


FIG. 12: Cooling Time for the PT30RM. The red line is the cold finger, the green line is the breadboard/beam splitter, the orange line is the inner shield, and the blue line is the outer shield

CryoCooler Name	CryoCooler Power @ 123 K	2 layers of shields with covers	2 layers of shields	1 layer of shields with covers	1 layer of shields	2 layers of shields with covers Cold
DS Min1	4.12	{ } : { } : { }	{ } : { } : { }	{ } : { } : { }	{ } : { } : { }	{ } : { } : { }
MT	12.6	29:38:20	30:06:4	30:52:13	31:28:10	211:14:13
CT	21.6	15:37:46	15:44:13	15:42:10	15:48:55	63:49:18
GT	30.75	11:37:17	11:40:50	11:38:38	11:42:17	47:62:6
DS 30	61.5	7:45:37	7:47:15	7:45:54	7:47:33	32:00:1
RD 125	50.	7:37:8	7:38:22	7:37:19	7:38:34	28:40:52
CH 104	63.6	6:25:26	6:26:21	6:25:32	6:26:28	24:43:52
CH 110	220.	4:41:42	4:42:16	4:41:44	4:42:18	19:11:41
AL 10	14.	27:40:8	27:52:8	27:57:11	28:10:14	100:32:43
AL 60	60.	6:25:14	6:26:7	6:25:20	6:26:13	24:20:58
PT 30	46.1143	7:50:23	7:51:53	7:50:38	7:52:9	31:12:13
PT 30-RM	39.1971	8:50:0	8:51:55	8:50:25	8:52:21	35:06:38
PT 60	60.	6:41:60	6:43:0	6:42:7	6:43:8	25:52:29
PT 63	22.	14:38:19	14:41:36	14:39:43	14:43:5	48:25:11
PT 90	90.	6:03:52	6:04:47	6:03:58	6:04:53	24:28:21
DE-102F	21.6712	15:16:59	15:21:38	15:19:35	15:24:24	56:42:20
DE-102(T) F	33.1918	10:10:21	10:12:33	10:10:56	10:13:9	38:21:32
DE-104F	44.4521	8:12:40	8:14:10	8:12:56	8:14:27	31:30:13
DE-104(T) F	78.9041	6:22:28	6:23:29	6:22:35	6:23:36	25:36:60
DE-110	200.	5:04:17	5:04:58	5:04:20	5:05:11	20:56:10
DE-202AE	4.	{ } : { } : { }	{ } : { } : { }	{ } : { } : { }	{ } : { } : { }	{ } : { } : { }
DE-202A(T) E	6.	184:48:14	193:12:7	{ } : { } : { }	{ } : { } : { }	{ } : { } : { }
DE-204AE	17.	20:44:33	20:51:19	20:50:14	20:57:18	72:29:40
DE-204A(T) E	23.	14:02:46	14:05:56	14:04:5	14:07:20	48:22:20
DE-204PE	14.	27:40:8	27:52:8	27:57:11	28:10:14	100:28:33
DE-210	25.	12:46:16	12:48:56	12:47:13	12:49:55	44:01:20
OC 0/12 60 rpm	13.	31:08:19	31:23:29	31:35:7	31:52:0	116:54:33
OC 0/12 90 rpm	18.	19:15:25	19:21:19	19:19:48	19:25:57	67:24:41
OC 0/40 60 rpm	50.	7:19:0	7:20:6	7:19:9	7:20:15	27:05:6
OC 0/40 90 rpm	62.	6:17:25	6:18:15	6:17:30	6:18:20	23:41:49
Power Lost to Bath at Equilibrium	N/A	5.29989	5.35781	6.42072	6.50522	8.31588

FIG. 13: Cooldown Time and Power Table for different Cryocoolers and shielding configurations. { } : { } : { } means the cryocooler isn't powerful enough for the beam splitter to reach 123 K